# The tautomer-specific excited state dynamics of 2,6-diaminopurine using REMPI and quantum chemical calculations

Gregory Gate,[1] Ann Williams,[1] Samuel Boldissar,[1] Jiří Šponer,[2,3] Rafal Szabla*[4] and Mattanjah de Vries*[1]

*[1.] Department of Chemistry and Biochemistry, University of California, Santa Barbara, California 93106-9510, USA., [2]. Institute of Biophysics of the Czech Academy of Sciences, 61265 Brno, Czech Republic, [3]. Regional Centre of Advanced Technologies and Materials, Czech Advanced Technology and Research Institute (CATRIN), Palacky University Olomouc, 783 71 Olomouc-Holice, Czech Republic, [4]. Institute of Advanced Materials, Faculty of Chemistry, Wrocław University of Science and Technology, 50-370 Wrocław, Poland*

*Corresponding author email: devries@chem.ucsb.edu (MS de Vries); rafal.szabla@pwr.edu.pl (R. Szabla)

## ABSTRACT

2,6-diaminopurine (2,6-dAP) is an alternative nucleobase that potentially played a role in prebiotic chemistry. We studied its excited state dynamics in the gas phase by REMPI, IR-UV hole burning, and ps pump-probe spectroscopy and performed quantum chemical calculations at the SCS-ADC(2) level of theory to interpret the experimental results. We found the 9H tautomer to have a small barrier to ultrafast relaxation via puckering of its 6-membered ring. The 7H tautomer has a larger barrier to reach a conical intersection and also has a sizable triplet yield. These results are discussed relative to other purines, for which 9H tautomerization appears to be more photostable than 7H and homosubstituted purines appear to be less photostable than heterosubstituted or singly substituted purines.

# INTRODUCTION

The current understanding of the photochemistry of isolated canonical nucleobases is that they are very photostable thanks to rapid internal conversion from the excited state to the electronic ground state. This deactivation mechanism protects the building blocks of the genetic code from possible photochemical damage by efficiently converting electronic excitation to heat that can be safely dissipated to the environment. (1-10) This process corresponds to excited state lifetimes of the order of single picoseconds or less. By contrast, many derivatives, isomers, and analogues of the canonical nucleobases have much longer excited state lifetimes, with competing and potentially hazardous photochemical pathways. (11, 12) These excited state dynamics are a subtle function of molecular structure. Although the picture is far from complete, there are some indications that heterosubstituted purines (*e.g.* guanine(13) and isoguanine(14)) may be more photostable than the homosubstituted purines (2,6-diaminopurine and xanthine(15, 16)), while purines with a single ligand (adenine,(17) 2AP,(18) 2-oxopurine,(19) and hypoxanthine(20)) appear to be more photostable than most purines with two ligands.(13) Martinez-Fernandez et al. in a thorough computational study on the photostability effects of position and oxo/amino substitution for purines with a single ligand,(19) found that amino or oxo substitution at $C_2$ has little effect on the photodynamics, while $C_6$ functionalization leads to photostability. However, these general trends do not include details, such as the role of the solvent.

A well-known example of this structure dependence is the difference between adenine (6-aminopurine), and its isomer 2-aminopurine (2AP). 2AP has a strong fluorescence signature in aqueous solution, while adenine does not. Adenine in the gas phase has an excited-state lifetime of the order of single picoseconds or less depending on the exact measurement technique,(4, 21-25) with similar lifetimes reported in solution.(26) The lowest excited singlet state of adenine exhibits $n\pi^*$ character and significant $^1n\pi^*/^1\pi\pi^*$ mixing after initial excitation.(26-31) Adenine undergoes aromatic ring puckering associated with $C_2$-H tilting and out-of-plane deformation at the $C_2N_3$ position to reach an $S_1/S_0$ conical intersection (CI) with a barrier of about 0.1 eV, enabling relaxation to the electronic ground state. In contrast, Lobsiger et al. found isolated 2AP to have an excited-state lifetime of 150 ps when excited near the excitation threshold, which is significantly longer than in the case of isolated adenine.(18) Furthermore, these authors observed another decay component with a lifetime of more than 2 μs, attributed to a triplet state populated by intersystem crossing. The lifetime increases significantly upon microhydration near the amino group in the $C_2$ position, i.e., up to a hundredfold compared to the isolated molecule. This increase presumably corresponds to the fluorescence decay noted for solvated 2AP.(32-35)

The excited-state dynamics also depends on the irradiation wavelength, especially near excitation threshold (origin transition) where dynamics can be slow. In that case the dynamics can be hypersensitive to any barriers, which can modulate competing relaxation pathways. For instance, at higher excitation energies, adenine can also relax via N-H bond breaking, which occurs in the $^1\pi\sigma^*$ state.(27-30, 36, 37) For isolated 2AP, the lifetime of 150 ps decreases by about half after exciting with ~1500 $cm^{-1}$ excess energy, relative to the origin.(18)

Structural motifs do not always predict trends in potential energy surfaces and effects of substitutions do not necessarily add up.(38) Potential energy surfaces are subtly influenced by molecular structure, and the photochemistry of 2,6DAP (see Scheme 1) cannot be simply understood as a combination of the pathways available for 2AP and 6AP. Therefore, to shed more light on the photodynamics of amino substituted purines, we have investigated the excited-state properties of isolated 2,6-dAP which has common structural features with both 2AP and adenine. The photochemistry of 2,6-dAP is also of interest since it has been suggested as a prebiotically relevant nucleobase; it was discovered in meteorite samples,(39) and it could be synthesized from the same starting materials and under the same conditions as the canonical nucleobases.(40) More recently, 2,6-dAP was shown to entirely replace adenine in the genomes of numerous bacterial viruses (bacteriophages).(41-43) In addition, its remarkable electron-donating properties were suggested to enable a potentially prebiotic version of DNA repair in UV-rich environments.(44) Because of these prebiotic and biological implications, thorough characterization of the photodynamics of 2,6-dAP is warranted. Here, we focus on studying both the biologically relevant 9H tautomer, and the 7H tautomer. In previous work(45), we found 6.3 and 8.7 ns lifetimes for the isolated 9H and 7H tautomers at their respective origins. These lifetimes stand out from those in both adenine (< 1 ps) and 2AP (150 ps and 2 μs). Now, to gain further insight, we investigated the dynamics of isolated 2,6-dAP in the picosecond time regime and found an additional fast decay pathway with different barriers for each tautomer. We discuss potential mechanisms that could explain the observed lifetimes based on quantum chemical calculations. By comparing our experimental and theoretical results with data previously acquired for adenine and 2AP, we attempt to reconcile the excited state dynamics with properties of the molecular structure.

# METHODS

## Experimental

The experimental setup has been described in detail elsewhere (46), and only a short description follows. 2,6-dAP (Aldrich, 98% purity) was placed on a translating graphite bar and desorbed by a focused Nd:YAG laser pulse (1064 nm, ~1 mJ/pulse at 10 Hz). A pulsed argon molecular beam (8 atm backing pressure, 30 μs pulse width) entrained the gaseous molecules in a supersonic jet expansion, quickly cooling them. Downstream, resonance enhanced multiphoton ionization (REMPI) ionized the cold, gaseous molecules and the ions entered into a reflectron time-of-flight mass spectrometer for detection.

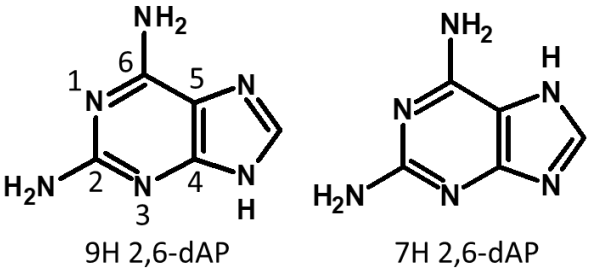


***Scheme 1.*** *9H (left) and 7H (right) tautomers of 2,6-diaminopurine*

We performed two-color resonant two-photon ionization (2C-R2PI) using an EKSPLA PL2251 Nd:YAG laser system producing ~30 ps pulses. The 355 nm output pumped a tunable optical parametric generator (OPG) (UV output of ~100 μJ). Leftover 1064 nm and 532 nm light from the pump were combined to generate the 5$^{th}$ harmonic at 213 nm (0.3 mJ), to be used as the ionization pulse. We also used the 193 nm output from a GAM excimer laser to ionize (2 mJ per pulse, 8 ns pulse width).

A Laser Vision tunable optical parametric oscillator/optical parametric amplifier (OPO/OPA) (mid-IR output 3200-3800 $cm^{-1}$, ~2 mJ/pulse, 3 $cm^{-1}$ spectral line width) generated IR light. The IR pulse preceded the excitation/ionization pulses by ~200 ns. We used two variations of IR double resonant spectroscopy. In mode I, the IR laser scanned across IR wavelengths, while the ionization pulse was held constant at a resonant R2PI transition for a given tautomer. When the IR pulse was resonant with a vibrational mode, it modified the ground state vibrational population, taking the excitation pulse out of resonance and causing a decrease in signal. This produced the IR spectrum for the specific tautomer that was being ionized. In mode II, the IR pulse was held constant at a resonant vibrational transition, while the excitation pulse scanned the R2PI spectrum. In this method, a tautomer was labeled by a vibrational stretch and signal decreased wherever the vibrational transition was shared. Digital chopping created control pulses by firing the IR pulse (pump pulse) 200 ns *after* the excitation/ionization pulses (probe pulses), generating ions that have not interacted with the IR light.

Pump-probe experiments measured lifetimes. The pump pulse from the OPG laser system was tuned to a resonant transition. The probe pulse, at 213 nm, was mechanically delayed up to 1.8 ns in time, relative to the OPG pulse. With ~30 ps pulse widths for both the pump and probe pulses, this allowed probing of dynamics in the ps regime. Alternatively, we conducted pump-probe mesurements using the OPG laser system for the pump and the excimer laser at 193 nm as the probe pulse, which was delayed electronically, allowing for much longer delays. Due to the 8 ns pulse width of the 193 nm pulses, this arrangement was blind to < 1 ns dynamics. Probing with 213 or 193 nm served as complementary techniques allowing us to observe both fast and slow dynamics.

The method for deriving lifetimes is based on previous work, and explained in more detail there.(47) Briefly, lifetimes are derived from kinetic equations, solving a system of ordinary differential equations. This approach involves convolving the instrument response function (IRF) with exponential decay functions. The IRF is represented by a Gaussian function centered around $t_{0,}$ corresponding to the pump and probe pulses overlapping in time.

## Quantum chemical calculations

We performed static explorations of excited-state potential energy surfaces using the spin-component scaling variant of the algebraic diagrammatic construction to the second order method (SCS-ADC(2)).(48, 49) The SCS-ADC(2) variant was recently shown to provide a more accurate description of excited-state energies and potential energy surfaces of heteroaromatic systems (e.g. nucleobases) when compared with the more standard ADC(2)-s approach.(50) Consequently, we performed all excited-state energy calculations and geometry optimizations at the SCS-ADC(2) level of theory, whereas ground-state energies and geometries were obtained with the equivalent SCS-MP2

approach. For all these calculations we also used the cc-pVDZ-F12 basis set, which although dedicated to explicitly correlated methods, was recently demonstrated to provide excited-state energies and properties with the accuracy of the aug-cc-pVTZ basis set or larger at a lower computational cost.(51) Notably, the cc-pVNZ-F12 basis sets contain more valence functions than included in the conventional cc-pVNZ series in addition to a minimal subset of diffuse functions, which ensure better convergence of Hartree-Fock energy as well as correlation energy, and better overall description of molecular properties.(51) The minimum-energy crossing points between different electronic states were optimized using the approach of Levine and coworkers and the SCS-ADC(2) and SCS-MP2 methods were used to calculate excited-state energies and gradients of the electronic excited states and the ground state, respectively.(52) In particular, previous work demonstrated that the optimizations of state crossings at the ADC(2)/MP2 level offered accurate geometries of $S_1(\pi\pi^*)/S_0$ minimum-energy crossing points in bioorganic chromophores, which are the primary state crossings considered in this work.(53, 54) Our target compound also does not contain any carbonyl groups, which were recently shown to hinder the correct description of the topography of S1/S0 state crossings with ADC(2) and related methods.(55) The excited-state potential energy (PE) profiles were constructed with linear interpolation in internal coordinates between the key stationary points on the potential energy surface, that is, the Franck-Condon regions, $S_1$ minima and $S_1/S_0$ minimum energy crossing points (MECPs). Only in the case of the C6-puckering mechanism of 9H 2,6-dAP, we performed a minimum-energy path calculation on the $S_1$ PE surface between the C2-puckered and C6-puckered $S_1$ minima, using the woelfling module of the Turbomole program (56) and the SCS-ADC(2)/cc-pVDZ-F12 level of theory. To further validate the accuracy of our SCS-ADC(2) calculations we performed single point energy calculations for five primary photorelaxation pathways and the associated potential energy surfaces using the NEVPT2/SA-CASSCF method and the def2-TZVP basis set. These results are presented in Fig. S9 in the ESI and the orbitals included in the active spaces are presented therein. Overall, the active space for all calculations of singlet photorelaxation mechanisms included 8 electrons correlated in 8 orbitals (4 occupied $\pi$ and 4 virtual $\pi^*$ orbitals), while for the triplet photorelaxation mechanism of the 7H tautomer of 2,6-dAP we applied a somewhat smaller active space including 8 electrons correlated in 6 orbitals (4 occupied $\pi$ and 2 virtual $\pi^*$ orbitals). These active spaces allowed us to maintain orbital populations between 0.02 and 1.98 and avoid orbital rotation for all studied photorelaxation pathways. Finally, the spin–orbit coupling (SOC) matrix elements between the S1 and T2 electronic states of 7H 2,6-dAP was computed with the CASPT2/SA-CASSCF method with 6 electrons correlated in 5 orbitals and the state-averaging procedure for lowest-energy singlet states and 3 lowest-energy triplet states. In order to account for scalar relativistic effects in our SOC calculations we applied the cc-pVTZ-DK basis set and the the 2$^{nd}$ order Douglas–Kroll–Hess Hamiltonian.(57, 58) All the SCS-ADC(2) and SCS-MP2 calculations were performed using the Turbomole 7.3 program(56), whereas we used the Molcas 8.4 program (59) for the CASPT2/SA-CASSCF calculations of SOC matrix elements.

## Results

### Experimental.

***Distinguishing the 7H and 9H tautomers of 2,6-dAP,*** An initial R2PI scan of 2,6-dAP served to identify resonant vibronic transitions. We observed two distinct regions of the spectrum, offset by ~2500 $cm^{-1}$ (see below). Using IR-UV mode I and mode II (see Figures S1-S3) we confirmed the presence of both the 7H and 9H tautomers, in accordance with earlier work by Gengeliczki et al.(45)

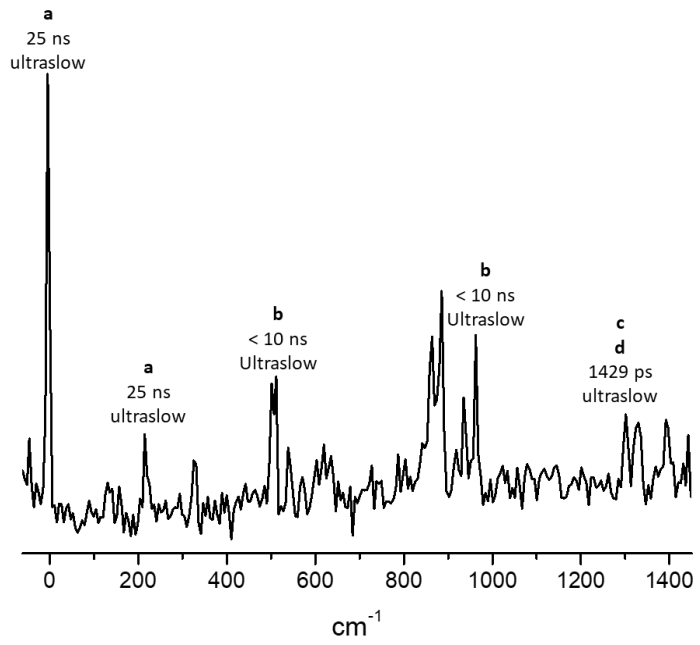


***Figure 1.*** *2C-R2PI spectrum of the 7H tautomer, obtained with ionization at 193 nm. Lifetimes are displayed above each peak. All lifetimes are from pump-probe measurements using the 193 nm probe with 8 ns pulses. The only exception is the 1429 ps lifetime, obtained using the 213 nm ps probe. Lifetimes were measured at the origin, 32216 $cm^{-1}$, and at +214, +511, +984, and +1307 $cm^{-1}$, relative to the origin. The letters correspond to peaks with similar pump-probe traces, shown in Figure 2.*

***2,6-dAP (7H) dynamics***, Figure 1 shows the 2C-R2PI spectrum of 2,6-dAP (7H). The origin transition is at 32216 $cm^{-1}$, which matches well with the origin found by Gengeliczki et al. (32215 $cm^{-1}$).(45) The R2PI spectrum was acquired using 193 nm as the second color. In addition, we acquired the R2PI spectrum for 7H 2,6-dAP using a picosecond ionization at 213 nm, which had similar features, but at worse signal to noise ratio (Fig. S1). This latter spectrum is generally more diffuse with no signal beyond 33600 $cm^{-1}$.

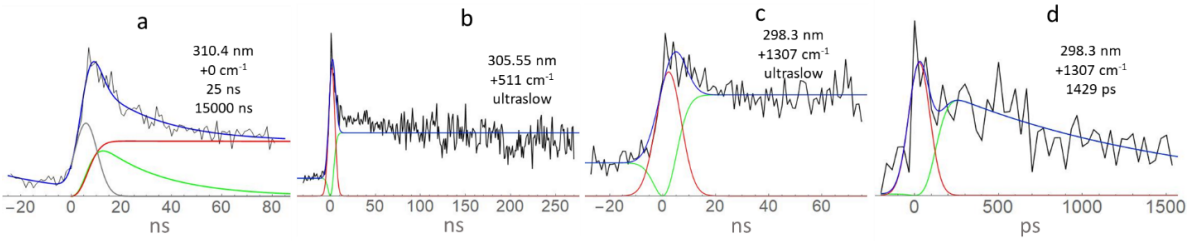


***Figure 2.*** *Sample pump-probe spectra of 2,6-dAP (7H). (a-c) were pumped with ps pulses and probed with ns 193 nm pulses. (d) was pumped with a ps pulse and probed with ps 213 nm. The origin and +214 cm$^{-1}$ (a) were fit with two exponentials while +511 and +984 cm$^{-1}$ (b) were fit with a monoexponential. +1307 cm$^{-1}$ (c,d) was fit with monoexponentials in the ns and ps regime. Note the change in x-axis units. Solid lines are calculated traces as follow: red and green traces represent different decay channels, black is the IRF, and blue is the total combined trace.*

Figs. S4 – S6 show pump-probe spectra; figure 2 shows samples of excited-state decays. The nanosecond decay traces for the origin and +214 cm$^{-1}$ peaks (denoted with letter a, Fig. 1) are similar and both were fit using biexponential functions (Fig. 2a). To fit these two peaks, we assigned 25 ns and 15000 ns time constants to exponential decay functions. While these fits are not unique, they represent a range of approximately ±25%.(60) The ps pump-probe traces for the +0 and +214 cm$^{-1}$ peaks show no indication of sub ns decay (Fig. S4). The origin decay differs from that measured by Gengeliczki et al.(45), in which we reported a single 8.7 ns lifetime. In that earlier work we used 266 nm for ionization. Using 193 nm in the current work allows ionization out of lower energy excited states, suggesting that the slow excited-state decay component that was not observed before, corresponds to a lower energy and much longer-lived triplet excited state.

Figure 2b shows a representative pump-probe spectrum for the two higher-energy peaks, at +511 and +984 cm$^{-1}$ denoted with letter b in Fig 1, using the 193 nm ns probe. We could not perform pump-probe measurements for these peaks using the picosecond probe pulses at 213 nm, due to low signal-to-noise. The spectrum in Fig. 2b, with its spike in the first 10 ns, corresponds to a combination of a very fast and a very slow decay. The fast decay has a lifetime equal to or smaller than the instrument response function (IRF) of approximately 10 ns. The slow channel can be fit with a single exponential decay with a lifetime of the order of 10 µs. Figures 2c and 2d show pump-probe spectra for the peak at +1307 cm$^{-1}$ (denoted with letter c in Fig. 1) with ns 193 nm and ps 213 nm probe pulses, respectively. The slow part of the nanosecond trace was fit with a monoexponential function just as in the case of the peaks denoted with letter b with a lifetime of the order of 10 µs. The picosecond probe pulse at 213 nm also allowed us to estimate the shorter-lived component with a lifetime of 1429 ps (Fig. 2d).

In summary, we observed two decay components for the 7H tautomer of 2,6-dAP. We recorded an ultraslow component for all peaks. In addition, we recorded a faster component with the time constants equal to 25 ns for the origin and +214 cm$^{-1}$ peaks. That component then becomes shorter with increasing pump energy, of the order of 1 – 10 ns for

the peaks at +511 and +984 $cm^{-1}$ and 1429 ps at +1307 $cm^{-1}$ with respect to the origin transition.

***2,6-dAP (9H) dynamics,*** Figure 3 shows the 2C-R2PI spectrum of the 9H tautomer from 34800 to 35650 $cm^{-1}$ acquired with ionization at 213 nm. We assign the band at 34885 $cm^{-1}$ to the origin transition of the 9H tautomer in agreement with our previous work.(45)This origin transition is higher in energy by ~ 2500 $cm^{-1}$ than the origin transition of the 7H tautomer. With increasing energy lifetimes shorten. Beyond ~500 $cm^{-1}$ excess energy lines broaden, and decrease in intensity, suggesting a further decrease of the excited state lifetime. The lifetime in the picosecond regime quickly decreases by an order of magnitude beyond +180 $cm^{-1}$, and then by another order of magnitude beyond +700 $cm^{-1}$, relative to the origin transition. Fig. 4 shows pump-probe traces for the origin and and for the +790 $cm^{-1}$ peak. All pump-probe traces and their fits are presented in Fig. S7.

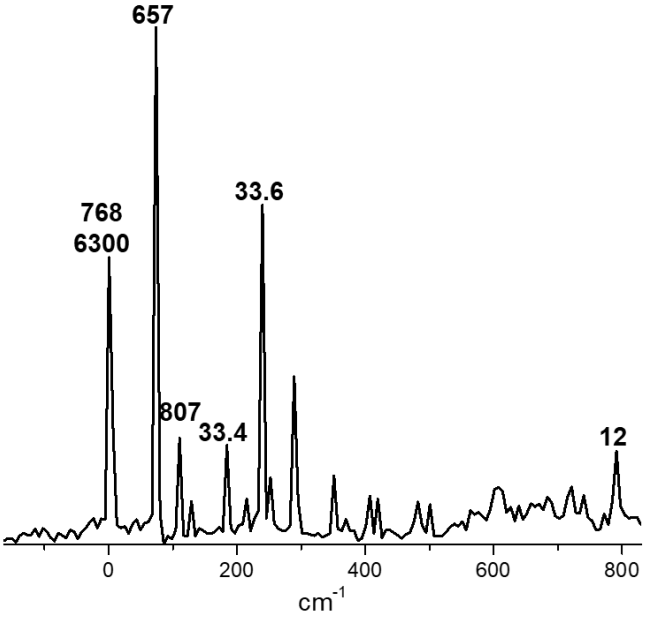


***Figure 3.*** *2C-R2PI spectrum of the 9H tautomer of 2,6-diaminopurine in the gas phase using the ps 213 nm as probe. The origin transition is assigned to 34885 $cm^{-1}$. Lifetimes are displayed above the corresponding peaks, in ps. The lifetime of 6300 ps was measured in the ns regime using the 193 nm probe and matches previously published measurements. Lifetimes were measured at the origin, 34885 $cm^{-1}$, and +73, +110, +183, +239, +790 $cm^{-1}$, relative to the origin.*

The 2C-R2PI spectrum, presented in Fig. 3, is in good agreement with the spectrum acquired by Gengeliczki et al(45) using ns 266 nm ionization. That previous 2C-R2PI spectrum for 9H 2,6-dAP becomes very diffuse with no clear peaks at excess energies higher than ~250 $cm^{-1}$. This cut-off value is in line with the faster dynamics that we observed in our measurements since the ionization efficiency decreases when the excited state lifetime becomes shorter than the pulse width of the ionization laser. We also performed a nanosecond pump-probe measurement at the origin peak, deriving a lifetime

of 6.3 ns. We assume that this nanosecond decay pathway exists for the first three peaks (+0, +73, +110 $cm^{-1}$), where the spectrum is still sharp. Broadening of higher energy peaks in the spectrum indicates that the photorelaxation of 9H 2,6-dAP occurs on a much faster timescale with excess energy above 180 $cm^{-1}$. This conclusion is also supported by much shorter picosecond time constants derived by fitting the pump-probe data for the three rightmost peaks presented in Fig. 3, namely 33.4 ps, 33.6 ps and 12.0 ps.

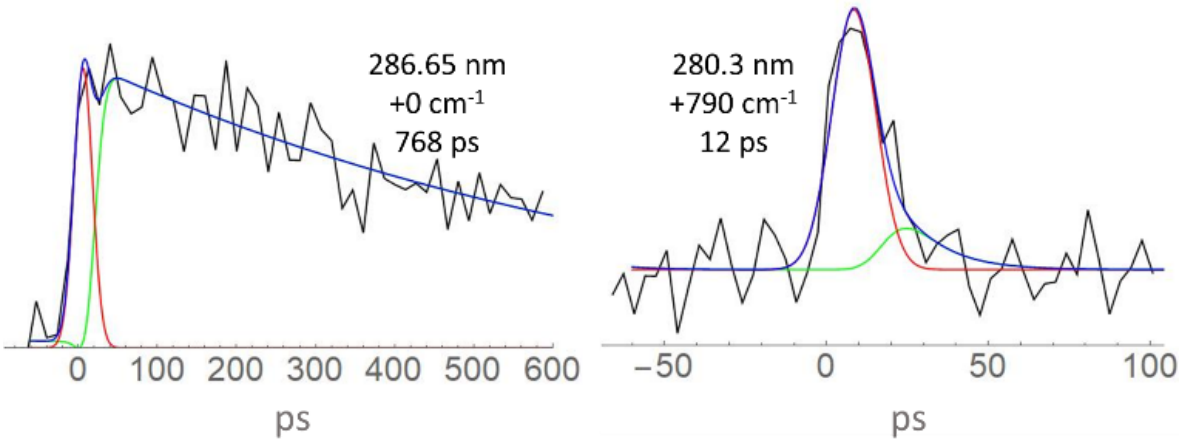


***Figure 4.*** *Pump-probe traces using ps 213 nm as probe for 2,6-dAP (9H). The left trace was obtained at the origin (34885 $cm^{-1}$) while the right trace was obtained at 35675 $cm^{-1}$.*

As we move to higher energies above the origin transition in the 2C-R2PI spectrum for 9H 2,6-dAP, the lifetime becomes progressively shorter. Starting at the origin, the first few peaks have lifetimes on the order of 750 ps, in addition to the ns component found earlier. These photodeactivation time constants are significantly larger than for adenine and 2AP. We found that the lifetime quickly drops to ~35 ps beyond about 180 $cm^{-1}$ excess energy for 9H 2,6-dAP. The last notably large and discrete peak, at +790 $cm^{-1}$ has a lifetime no longer than 12 ps. The picosecond excited-state decays are most likely associated with radiationless deactivation pathways. Meanwhile, the nanosecond decay might originate from a fluorescence pathway.

## Computational

***Vertical excitation energies.*** Table 1 lists vertical excitation energies calculated for both 7H and 9H tautomers of 2,6-dAP at the SCS-ADC(2) level of theory. In the case of these tautomers, the lowest energy excitation is dominated by the ππ* molecular orbital character and characterized by a relatively high oscillator strength. It is also worth adding that these optically bright ππ* excitations are energetically well separated from higher-energy excited states. This indicates that excitation of 2,6-dAP with low energy photons, e.g. near the 0-0 transition or lowest energy absorption maxima will likely entail photodeactivation mechanisms characteristic of ππ* excited states, e.g. ring puckering. Therefore, we anticipate that the photorelaxation of 2,6-dAP observed in our experimental setup is

primarily associated with these excitations. According to our SCS-ADC(2) results, the $S_1(\pi\pi^*)$ state of 7H 2,6-dAP is lower in energy than the analogous excitation in the 9H tautomer by 0.35 eV, i.e. 4.47 eV vs. 4.83 eV respectively.

***Table 1.*** *Vertical excitation energies of the 7H and 9H tautomers of 2,6-dAP calculated at the SCS-ADC(2)/cc-pVDZ-F12 level of theory, using ground-state geometries optimized with the MP2 method and the same basis set.*

| 7H tautomer of 2,6-dAP | | | | |
|---|---|---|---|---|
| State | Character | $E_{exc}$ [eV] | $f_{osc}$ | λ [nm] |
| $_{S1}$ | $\pi\pi^*$ | 4.47 | 0.121 | 277.5 |
| $S_2$ | $\pi\sigma^*_{NH}$ | 5.03 | $3.70 \times 10^{-3}$ | 246.7 |
| $S_3$ | $n\pi^*$ | 5.19 | $2.66 \times 10^{-3}$ | 238.8 |
| $S_4$ | $\pi\pi^*/\pi\sigma^*_{NH}$ | 5.59 | 0.012 | 221.9 |
| $S_5$ | $\pi\sigma^*_{NH}$ | 5.69 | 0.024 | 217.9 |
| $S_6$ | $\pi\sigma^*_{NH}$ | 5.98 | 0.032 | 207.4 |
| 9H tautomer of 2,6-dAP | | | | |
| $_{S1}$ | $\pi\pi^*$ | 4.83 | 0.140 | 256.8 |
| $S_2$ | $\pi\sigma^*_{NH}$ | 5.35 | 0.015 | 231.8 |
| $S_3$ | $\pi\pi^*$ | 5.39 | 0.185 | 229.8 |
| $S_4$ | $n\pi^*$ | 5.61 | $2.44 \times 10^{-3}$ | 220.8 |
| $S_5$ | $\pi\sigma^*_{NH}$ | 5.71 | $7.19 \times 10^{-3}$ | 217.3 |
| $S_6$ | $\pi\sigma^*_{NH}$ | 5.90 | 0.019 | 210.2 |

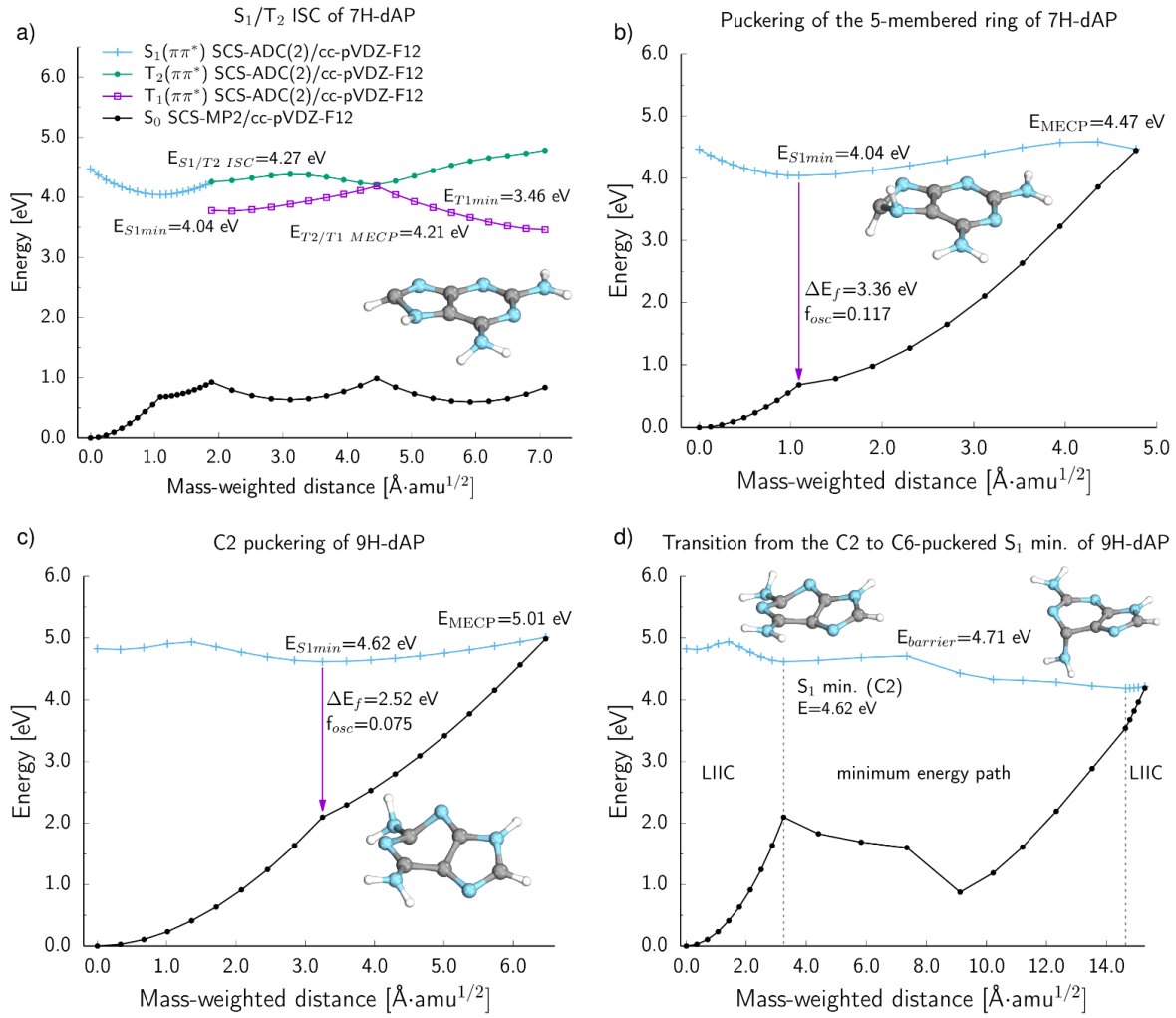


***Figure 5***. *Potential energy profiles presenting different photorelaxation pathways (mechanisms) of the 7H (a and b) and 9H (c and d) tautomers of 2,6-dAP with the excited-state energies calculated at the SCS-ADC(2)/cc-pVDZ-F12 level of theory and energies of the ground state calculated at the SCS-MP2/cc-pVDZ-F12 level of theory. The profiles were constructed by linear interpolation in internal coordinates (LIIC) between the Franck-Condon region and respective excited-state minima and state crossings. Only in the case of panel d), part of the PES was computed as a minimum energy path between the C2-puckered and C6-puckered S1 minima of the 9H tautomer. The inserted structures correspond to the $T_1$ minimum (panel a), $S_1/S_0$ minimum-energy crossing points (panels b, c and d on the right). The inserted structure on the left-hand side of panel d corresponds to the $S_1$ minimum.*

Both 7H and 9H tautomers are also characterized by low-lying $S_2(\pi\sigma^*_{NH})$ states for which the repulsive σ* orbital is centered around the $N_7$-H or $N_9$-H bond in the five-membered ring of 2,6-dAP. While these states could directly contribute to the photorelaxation of 2,6-dAP even at low excitation energies, photodissociation of N-H bonds is an ultrafast process occurring on the timescale of tens to hundreds of fs (61, 62)

and, thus, is below the probe resolution of our experiments. Furthermore, in our experiment we only observed parent masses. The $S_3$ state of 7H 2,6-dAP is dominated by the nπ* electronic configuration, which is analogous to the nπ* state of 9H adenine. However, we expect this state to play a minor role in the photodynamics of 2,6-dAP excited near the 0-0 transition, owing to the excitation energy of this nπ* state being 5.19 eV. Similarly, the corresponding nπ* of the 9H tautomer of 2,6-dAP is even higher in energy (5.61 eV) and assigned to the $S_4$ state according to our calculations. Nevertheless, the nπ* states might play a role in the photodeactivation of 2,6-dAP at higher absorption energies, which were not considered in this work.

***Excited-state geometry optimizations.*** Excited-state geometry optimizations and SCS-ADC(2) calculations of potential energy profiles connecting the key stationary points and state crossings provide further insights into the photodeactivation mechanisms that can be attributed to the measured excited-state lifetimes of 2,6-dAP. In particular, the adiabatic excitation energies of the $S_1$ states (energy difference between the $S_1$ and $S_0$ minimum energy geometries) of the 7H and 9H tautomers are in good agreement with the measured origins of absorption. The calculated adiabatic excitation energy of the $S_1$ state of 7H 2,6-dAP amounts to 4.04 eV, which is in semi-quantitative agreement with the measured origin of absorption of 3.99 eV. In the case of the 9H tautomer the corresponding theoretical and experimental values amount to 4.62 eV and 4.33 eV, respectively. Though the energy difference is larger, the theoretical result is well within the error bars of the ADC(2) method (63) and the qualitative trend is retained, in the sense that 9H 2,6-dAP has clearly higher adiabatic excitation energy of the $S_1$ state. Using the $S_1$ minimum energy geometries and different minimum-energy crossing points found at the SCS-ADC(2)/SCS-MP2 level of theory, we constructed several potential energy profiles which can be assigned to different excited-state lifetimes derived from our pump-probe measurements, discussed below.

***Photorelaxation of the 7H tautomer,*** As presented in Fig. 5, both tautomers of 2,6-dAP undergo structural changes after population of the $S_1$ state, with aromatic ring-puckering mechanisms being the most apparent structural changes that can be observed for both $S_1$ minima. The $S_1$ minimum-energy geometry of the 7H tautomer has a strongly puckered 5-membered subunit of the aromatic purine ring, which is the result of $C_8$=$N_7$ bond twisting. Population of this minimum may be followed either by intersystem crossing to the triplet manifold of electronic states or by direct internal conversion to the electronic ground state via the $S_1(\pi\pi^*)/S_0$ conical intersection (see Fig. 5 a and b). Direct photorelaxation via the $S_1(\pi\pi^*)/S_0$ conical intersection involves stronger puckering of the 5-membered heteroaromatic subunit and is associated with an energy barrier of over 0.4 eV. The presence of this energy barrier is consistent with the experimentally determined lifetime of 25 ns at excitation energies near the origin of absorption. This time constant is substantially shortened when the excess energy of the laser pulse reaches 1300 $cm^{-1}$, which is also in good qualitative agreement with the magnitude of computationally predicted barrier height. These considerations clearly indicate that the nanosecond time constant can be associated with a radiationless deactivation pathway. We cannot exclude the contribution from fluorescence though which occurs on a similar time-scale and could operate from the $S_1(\pi\pi^*)$ minimum of 7H 2,6-dAP, owing to the relatively high oscillator strength (0.117) of the radiative $S_1$-$S_0$ transition.

Due to the relatively long timescale of direct internal conversion through the $S_1(\pi\pi^*)/S_0$ conical intersection, UV-excited 7H 2,6-dAP may also undergo intersystem crossing to the triplet manifold of electronic states. Notably, the energy difference between the $S_1/T_2$ state crossing and the $S_1(\pi\pi^*)$ minimum amounts to merely 0.23 eV. Crossing to the triplet state from the $S_1$ minimum is only slowed down by the very low value of spin-orbit coupling (SOC) between these two electronic states of 1.92 cm-1. This very low degree of SOC is caused by the fact that the S1 and T2 states possess a very similar $\pi\pi^*$ molecular orbital character, albeit with different molecular orbitals defining these excitations. However, we argue that this intersystem crossing could still enable non-negligible population of triplet states. It is worth noting that based on MS-CASPT2/SA-CASSCF calculations, Oliveira et al. identified a likely more efficient intersystem crossing channel involving the T2($n\pi^*$) which is also associated with a higher S1/T2 SOC of ~10 cm-1. As can be seen from Fig. 5a, the minimum of the T1 state can be reached in a practically barrierless manner after the intersystem crossing, via the peaked T2/T1 conical intersection. Overall, these two intersystem crossing channels, confirmed computationally, allow us to tentatively assign the ultralong microsecond time constant to the population of the $T_1$ state. Even though the $T_1$ minimum of 7H 2,6-dAP exhibits an analogous molecular orbital character to the above-discussed $S_1$ minimum, it is also characterized by a somewhat lower degree of puckering of the 5-membered heteroaromatic subunit and lower degree of $C_8{=}N_7$ bond twisting.

***Photorelaxation of the 9H tautomer.*** In contrast to the 7H tautomer, the photodeactivation of 9H 2,6-dAP from its lowest energy singlet excited state is governed by puckering of the 6-membered subunit of the aromatic purine ring. In particular, the $S_1(\pi\pi^*)$ minimum of 9H 2,6-dAP is characterized by pyramidalization of the $C_2$ atom. From the $S_1$ minimum, the experimental results indicate the existence of two possible relaxation pathways with a faster internal conversion through a $S_1/S_0$ CI corresponding to the ps decay component competing with a slower pathway corresponding to the ns decay component. The extent of this pyramidalization and aromatic ring puckering is increased when the molecule approaches the $S_1(\pi\pi^*)/S_0$ conical intersection (see Fig. 5c). This state crossing lies nearly 0.4 eV higher in energy than the corresponding $S_1(\pi\pi^*)$ minimum and explains the long photodeactivation time constant, which amounts to 6.3 ns. We emphasize that owing to a relatively high oscillator strength of the $S_1$-$S_0$ transition from the $S_1(\pi\pi^*)$ minimum, this time constant could indeed be associated with fluorescence when the 9H tautomer is excited at the absorption origin. Alternatively, UV-excited 9H 2,6-dAP could undergo a change in the puckering mode associated with substantial rotation of the $C_6$-$NH_2$ amino group out of the plane of the aromatic purine ring and reach another ring-puckered $S_1(\pi\pi^*)/S_0$ conical intersection (see Fig. 5d). While this latter process is associated with an energy barrier of merely 0.1 eV, it also requires fitting of a picosecond excited-state decay component for the 9H tautomer.

***Possible photorelaxation mechanisms outside of our experimental window.*** In addition to the photorelaxation pathways which match our experimental observations, we have identified two other radiationless deactivation mechanisms of 2,6-dAP, that fall outside of our experimentally observable parameters. Similarly to the 9H tautomer, UV-excited 7H 2,6-dAP could undergo ring-puckering of the six-membered subunit of the aromatic purine

ring, involving pyramidalization of the C2 carbon atom (see Fig. 6a). According to our calculations, the associated $S_1$ minimum lies approximately 0.6 eV higher in energy than the origin transition (and the energy of our pump pulse) and is very unlikely to be populated in our experiments. Note that the geometry of this $S_1(\pi\pi^*)$ minimum is mainly associated with the puckering of the 6-membered aromatic subunit on the C2 atom, in contrast to the puckering of the 5-membered aromatic subunit in the case of the primary $S_1$ minimum of 7H 2,6-dAP discussed in the previous section. In addition, the corresponding $S_1(\pi\pi^*)/S_0$ conical intersection is also higher in energy than the $C_2$-puckered $S_1$ minimum and has a clearly sloped topography. Nevertheless, this alternative photorelaxation channel of the 7H tautomer could be triggered at higher excitation energies than those in our experiments.

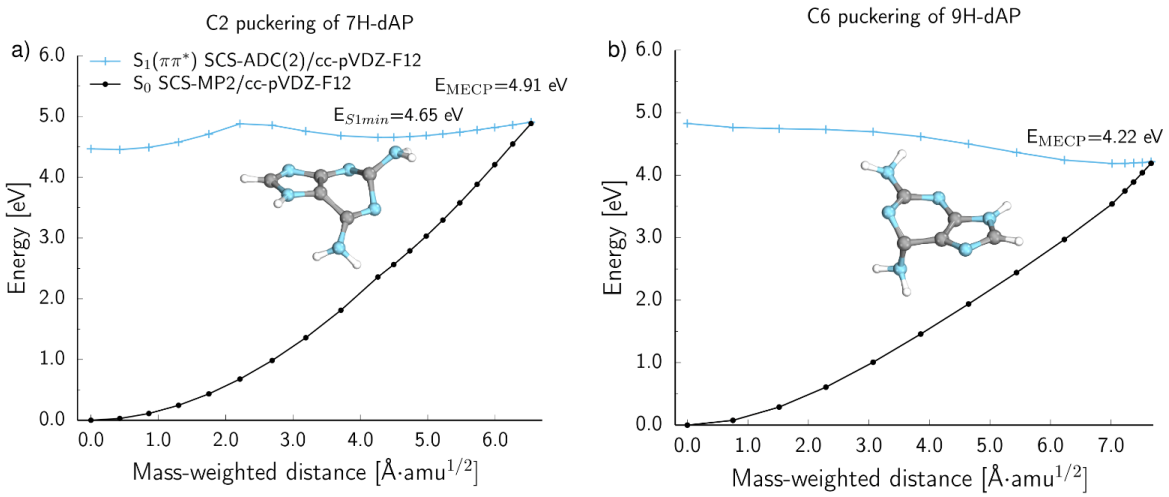


***Figure 6.*** *Potential energy profiles for the photorelaxation pathways of the 7H (panel a) and 9H (panel b) tautomers of 2,6-dAP calculated with the excited-state energies calculated at the SCS-ADC(2)/cc-pVDZ-F12 level of theory and energies of the ground state calculated at the SCS-MP2/cc-pVDZ-F12 level of theory. The inserted structures correspond to $S_1/S_0$ minimum-energy crossing points (MECPs).*

The 9H tautomer may also undergo a direct and entirely barrierless radiationless photodeactivation leading directly from the Franck-Condon region to a peaked $S_1(\pi\pi^*)/S_0$ conical intersection (see Fig. 6b). This process is driven by the aromatic purine ring puckering at the $C_6$ carbon atom alongside substantial twisting of the $C_6$-$NH_2$ amino group and is a more direct way of accessing this conical intersection. Since such barrierless excited-state ring-puckering processes were shown to occur in nucleobases on a sub-picosecond timescale,(64) this mechanism is most likely much faster than the resolution of our probe pulse and we would not be able to record it with our experimental setup. Nevertheless, we expect this mechanism to be an important contributor to the overall photorelaxation of 9H 2,6-dAP, even when excited near its absorption origin.

***Comparison of the SCS-ADC(2) results with previous computational studies of the photorelaxation mechanisms of 2,6-dAP*** Oliveira et al. recently published a comprehensive description of the photorelaxation mechanisms of 7H and 9H 2,6-diaminopurine based on MS-CASPT2/SA-CASSCF geometry optimizations and calculations of excited-state potential energy profiles. In particular, the authors located C2-puckered and C6-puckered $S_1/S_0$ state crossings for both tautomers, which are analogous to the C2- and C6-puckered $S_1/S_0$ state crossings discussed in this work. (65)

The MS-CASPT2/SA-CASSCF approach should generally offer a more accurate description of excited-state potential energy surfaces and $S_1/S_0$ state crossings, particularly in the regions where the ground-state wave-function gains a highly multi-configurational character. Therefore, we performed single point calculations at the NEVPT2/SA-CASSCF/def2-TZVP level to validate the potential energy profiles obtained with the SCS-ADC(2) method. As presented in Fig. S9, the SCS-ADC(2) results are in excellent qualitative agreement with the NEVPT2 energies and the primary quantitative difference between the two datasets is associated with a systematic shift of the PE profile obtained with the NEVPT2 approach to higher energies. Furthermore, the positions and geometries of the $S_1/S_0$ conical intersections were correctly identified with the SCS-ADC(2)/SCS-MP2 approach. Consequently, the $S_1/S_0$ conical intersection associated with the puckering of the 5-membered subunit of the purine aromatic ring of 7H 2,6-dAP is a possible photorelaxation mechanism, which was not identified in the previous study by Oliveira et al. Further, we have corroborated their finding of the C6-puckering mechanism for 7H 2,6-dAP. We located a virtually identical geometry of the C6-puckered $S_1/S_0$ MECP of 7H 2,6-dAP at the SCS-ADC(2)/SCS-MP2 level, and the associated potential energy profile exhibits an analogous high energy barrier (of 0.8 eV above the $S_1$ minimum) exceeding the vertical excitation energy of the $S_1$ state. It is worth noting though that we were not able to identify the $S_1$ minimum of 9H 2,6-dAP having the mostly planar geometry of the purine ring and the C6-NH2 group tilted by merely 28° with the SCS-ADC(2) method. We argue that SCS-ADC(2) likely overestimates the steepness of the S1 PE surface of 9H 2,6-dAP along the C6-puckering coordinate. Indeed, the corresponding NEVPT2 energies suggest a much flatter topography of this $S_1$ PE surface in the vicinity of the Frank-Condon region, which is indicative of the presence of another $S_1$ minimum which cannot be reproduced at the SCS-ADC(2) level. At the same time, the NEVPT2 results corroborate the feasibility of the ballistic C6-puckering mechanism of 9H 2,6-dAP, which can bypass this minimum and result in ultrafast photodeactivation as presented in Fig. 6b. In other words, the C6-puckered $S_1/S_0$ conical intersection of 9H 2,6-dAP can be reached in a barrierless manner from the Franck Condon region.

Our finding of the barrierless ballistic C6-puckering mechanism of photoexcited 9H 2,6-dAP is inconsistent with the calculations performed by Oliveira et al., who found a high barrier with a peak exceeding the vertical excitation energy of the ππ* La state by 0.08 eV. However, similar to our results, the C6-puckered $S_1/S_0$ conical intersection of 9H 2,6-dAP obtained at the MS-CASPT2/SA-CASSCF level is also lower in energy than the vertical excitation energy ot the ππ* La state. It is also important to emphasize that Oliveira et al. incorrectly associated this energy barrier with the barrier of 400 $cm^{-1}$ (0.05 eV) observed in our experiments. Specifically, our measurements allowed us to estimate the barrier above the 0-0 transition of 9H 2,6-dAP, which can be associated with the adiabatic

excitation energy of the $S_1$ state of the molecule and not with the vertical excitation energy as interpreted by Oliveira et al. The actual barrier height computed by Oliveira *et al.* amounts to 0.57 eV above the energy of the 0-0 transition, which substantially exceeds the measured value. Finally, to reiterate, since we were able to demonstrate this barrierless C6-puckering mechanism at the NEVPT2/SA-CASSCF level, we anticipate that the presence of this high energy barrier in the calculations performed at the MS-CASPT2/SA-CASSCF level might be an artifact of the geodesic interpolation procedure, which should be validated in the future.

As noted above, the MS-CASPT2/SA-CASSCF method also allowed Oliveira et al. to identify a more efficient intersystem crossing channel with higher SOC between the $S_1$ and $T_2$ states. Overall, the PE profiles presented in this work are complementary to the photorelaxation mechanisms proposed by Oliveira et al. In particular, we were not able to locate the planar C6-puckered minimum of 9H 2,6-dAP and the more efficient $S_1/T_2$ intersystem crossing of 7H 2,6-dAP. However, we identified C2-puckered $S_1$ minima and the associated photorelaxation mechanisms for both tautomers, located the $S_1/S_0$ state crossing associated with the puckering of the 5-membered subunit of the purine aromatic ring of 7H 2,6-dAP and demonstrated the feasibility of the ballistic C6-puckering photorelaxation mechanism of 9H 2,6-dAP.

***Table 2.*** *Spectral and lifetime data on purine and amino substituted purines.*

| | Tautomer | Origin [$cm^{-1}$] | $\tau_{0\text{-}0}$ [ps] | Range [$cm^{-1}$] sharp | broad | References |
|---|---|---|---|---|---|---|
| Purine | 9H | 31,309 | long | 2000 | - | (86, 66) |
| Adenine<br>6AP | 9H<br>7H | 36,101<br>35,824 | 9; 1 *<br>Unmeasured | 500 | - | (17);(26, 87)<br>(88) |
| 2AP | 9H<br>7H | 32,371<br>30,723 | 150<br>Unmeasured | 700<br>600 | 2000<br>200 | (18, 89)<br>(69) |
| Guanine | 9H | Unmeasured | Unmeasured | - | - | - |
| 2,6-dAP | 9H<br>7H | 34,881<br>32,215 | 655 / 6,300<br>25000/ultralong | 400<br>1000 | 800<br>800 | this work<br>this work |
| 2,4-dAPy | | 34459 | 766 | 350 | 300 | (45, 67) |

** at 37500 $cm^{-1}$*

## Discussion

## 7H tautomer:

We propose two distinct parallel relaxation mechanisms for the 2,6-dAP (7H) tautomer. (i) The initially bright $^1\pi\pi^*$ state of the 7H tautomer can decay directly to the ground state via puckering of the 5-membered subunit or by fluorescence, on the order of 25 ns. (ii) Alternatively, 7H 2,6-dAP can undergo intersystem crossing (ISC) to $T_2(^3\pi\pi^*)$. The relative yields do not appear to depend on excitation wavelength, based on the relative amplitudes of the decay traces (Fig. 2).

## 9H tautomer:

The relaxation model for 2,6-dAP (9H) also begins with population of a bright $^1\pi\pi^*$ state. A barrier on the order of 400 $cm^{-1}$ prevents the system from undergoing ultrafast nonradiative decay through a $^1\pi\pi^*/S_0$ CI. Therefore, some amount of the wavepacket will relax possibly via fluorescence at the $S_1$ minimum while the remainder eventually finds its way to a nonradiative decay channel by puckering at the $C_6$-$NH_2$ group (Fig. 5d). With increased excitation energy, no amount of fluorescence is observed, presumably outcompeted by the more efficient nonradiative decay.

Table 2 summarizes the spectral and lifetime data of the amino substituted purines in the gas phase, including the ranges of the 2C-R2PI spectra of each molecule within which one can observe sharp features and broad features. The lifetime of unsubstituted purine has not been reported in the gas phase. Previous pump-probe experiments performed for purine in acetonitrile and in aqueous solution reported lifetimes of singlet excited states which amount to 360 and 645 ps, respectively.(11) This singlet photorelaxation of unsubstituted purine is then followed by population of the lowest-energy triplet state with a quantum yield of approximately 0.9 with a much longer excited-state lifetime.(11) However, these measurements were performed in solution at significant excess energy relative to the origin transition. Meanwhile in the gas-phase, Schneider et al. reported a narrow rotational envelope of the origin peak, indicating a long lifetime(66) Thus, we can safely assume that purine has a relatively long lifetime in the gas phase. Therefore, the primary chromophore, the purine substructure, is not the reason for adenine's and guanine's photostability, which instead is due to their ligand substructures, a conclusion shared by ref (11). However, the effects of amino and oxo C2 and C6 substitutions are not additive and the mechanisms for each combination need to be individually described(38). This conclusion is in line with the work of Martinez-Fernandez et al. who examined how addition of a single amino or oxo group affects photostability and derived a mechanistic understanding of this effect(19). Their study is limited to purines with a single substituent, as doubly-substituted purines further complicate their mechanism. The current study builds on those findings with the diamino substitution adding another datapoint to the palette of substituent combinations.

2,4-diaminopyrimidine (2,4-dAPy) is the pyrimidine analogue of 2,6-dAP. From rotational contour fitting, we previously found it to have a lifetime between 10-1000 ps (45). Nachtigallova et al.(67) and Kancheva et al.(68) calculated the relaxation of 2,4-dAPy to be hindered due to a barrier while 4-aminopyrimidine (4-APy), the pyrimidine analog of adenine, is expected to exhibit ultrafast decay. We experimentally corroborated this finding for 2,4-dAPy, measuring a 766 ps lifetime near the origin (Fig. S7). Singly-substituted 4-APy can access ring-puckering CIs at $C_2$ at low excess energy and has a short lifetime,

like adenine. Meanwhile, the doubly-substituted 2,4-dAPy has some of these CIs hindered due to the second amino group, similar to dynamics in 2,6-dAP.

From this exploration of the photorelaxation mechanisms of 2,6-dAP, a few conclusions can be drawn about the relationship between purine structure and excited state dynamics. The increased photostability of the 2,6-dAP 9H tautomer compared to the 7H tautomer is in line with the photostability of the adenine tautomers both in the gas phase and in solution.(21, 25) The 9H tautomer origin transition ($^1\pi\pi^*$) in the gas phase tends to be to the blue of the 7H tautomer, for the handful of examples that are available (see table 1). The origin position is a direct measurement of the adiabatic energy of the $\pi\pi^*$ state. The relative energy levels of the $\pi\pi^*$ state versus the nearest $n\pi^*$ states affect the excited state dynamics, as shown with 2AP.(18, 69) With a few exceptions (guanine(13), isoguanine(14), and hypoxanthine(20)), it appears most purines (adenine, (26-31) 2AP(18), 2-oxopurine(19), xanthine(15, 16), purine(11)) and pyrimidines (cytosine(70), thymine(71, 72), and uracil(73)) relax from their initially excited $\pi\pi^*$ to an $n\pi^*$ to the ground state. Instead, 2,6-dAP follows the $^1\pi\pi^*/S_0$ CI path exclusively for 9H and both $^1\pi\pi^*/S_0$ internal conversion and $^1\pi\pi^*/^3\pi\pi^*$ ISC for 7H. The only difference between the two forms is the placement of the hydrogen on $N_7$ vs $N_9$ and this minor difference in structure has a significant effect on the excited state dynamics.

Caldero-Rodriguez et al. reported on the excited state dynamics of 2,6-dAP in solution, complemented with quantum calculations using implicit solvent.(10) Qualitatively, their experimental results for the 9H tautomer agree with ours, observing a fluorescent signature, and a nonradiative internal conversion pathway on the picosecond timescale. The authors assign the longer (1.8 ns) decay to fluorescence of the 7H tautomer, in line with previous fluorescence studies(74, 75), while we assign the much longer-lived excited state of the 7H tautomer to a triplet state. That work also observes a decay on the order of 0.7 ps, which is outside our experimental window. Similarly to the present study, Caldero-Rodriguez et al. calculate intersystem crossing to two lower-lying $^3\pi\pi^*$ states to be inefficient. Their calculations predict a barrierless internal conversion pathway along a $C_6$ conical intersection and another conical intersection via $C_2$ puckering with a less than 1 eV barrier for both tautomers. Our results agree with these findings, but we additionally found a conical intersection from puckering of the 5-membered ring (7H tautomer). Bearing in mind that those experiments were done in solution and at different wavelengths and that those calculations were done using implicit solvent, those findings correlate well with our gas-phase study.

Comparison of the dynamics of 2,6-dAP, purine, adenine, 2AP, and guanine shows a complex dependence on structure. Purine, the base structure, has a long excited state lifetime due to significant ISC(11, 66, 76, 77). Addition of a single amino group to $C_6$ forms adenine (6-aminopurine) with ultrafast nonradiative decay via $^1\pi\pi^* \rightarrow {}^1n\pi^* \rightarrow S_0$ and without any measurable triplet yield(17, 27, 29, 78-80). Adding an amino group to purine at $C_2$ forms 2AP with slower relaxation than adenine(18). 2AP also yields a sizable triplet population in the gas phase and in nonpolar solvent.(18, 33) This juxtaposition has suggested that the substitution of $C_2$ determines photostability(34, 78, 81). However, in 2AP, adding an oxo group to $C_6$ forms guanine, which leads to ultrafast nonradiative decay via a $^1\pi\pi^*/S_0$ conical intersection.(13, 82-85). Switching the oxo group on $C_6$ of guanine with an amino group leads to 2,6-dAP, which in the 9H form we found to follow the same

path as guanine (13). In the 7H form 2,6-dAP further has a triplet yield, in similar fashion as 2-oxopurine.(19) Even though 2,6-dAP shares structural elements with both 2AP and adenine, it does not have the same dynamics as either. 2,6-dAP is also the least photostable of these purines with the possible exception of purine itself. Photodynamics is intricately tied to structure, not only for ligand substitution, but also for tautomerization(1, 7, 12). With some data points in the purine structural family still missing, these results help shed light on the almost unique photostability of the canonical nucleobases and will hopefully lead to a more mechanistic understanding of the subtle interplay between structure and excited state dynamics.

## ACKNOWLEDGEMENTS

This work has been supported by the National Science Foundation under CHE-2154787 and by a grant from the National Science Centre, Poland (2020/37/B/ST4/04092 to R.S.). JS acknowledges support by the Czech Science Foundation (21-23718S).

## SUPPLEMENTARY MATERIALS

12 supplementary figures are provided

## REFERENCES

1. Gustavsson, T., R. Improta and D. Markovitsi (2010) DNA/RNA: Building Blocks of Life Under UV Irradiation. *J. Phys. Chem. Lett.* **1,** 2025-2030.

2. Middleton, C. T., K. de La Harpe, C. Su, Y. K. Law, C. E. Crespo-Hernandez and B. Kohler (2009) DNA Excited-State Dynamics: From Single Bases to the Double Helix. *Annual Review of Physical Chemistry* **60,** 217-239.

3. de Vries, M. S. (2008) Isolated DNA Base Pairs, Interplay Between Theory and Experiment. In *Radiation Induced Molecular Phenomena in Nucleic Acids*. (Edited by M. K. Shukla and J. Leszczynski), pp. 323-341. Springer Science+Business Media B.V.

4. Canuel, C., M. Mons, F. Piuzzi, B. Tardivel, I. Dimicoli and M. Elhanine (2005) Excited states dynamics of DNA and RNA bases: Characterization of a stepwise deactivation pathway in the gas phase. *Journal of Chemical Physics* **122,** 074316-074317.

5. Kang, H., K. T. Lee, B. Jung, Y. J. Ko and S. K. Kim (2002) Intrinsic lifetimes of the excited state of DNA and RNA bases. *Journal of the American Chemical Society* **124,** 12958-12959.

6. Sponer, J., J. Leszczynski and P. Hobza (2001) Hydrogen bonding, stacking and cation binding of DNA bases. *THEOCHEM* **573,** 43-53.

7. Beckstead, A. A., Y. Y. Zhang, M. S. de Vries and B. Kohler (2016) Life in the light: nucleic acid photoproperties as a legacy of chemical evolution. *Physical Chemistry Chemical Physics* **18,** 24228-24238.

8. Pecourt, J. M. L., J. Peon and B. Kohler (2001) DNA excited-state dynamics: Ultrafast internal conversion and vibrational cooling in a series of nucleosides. *Journal of the American Chemical Society* **123,** 10370-10378.

9. Improta, R., F. Santoro and L. Blancafort (2016) Quantum Mechanical Studies on the Photophysics and the Photochemistry of Nucleic Acids and Nucleobases. *Chemical Reviews* **116,** 3540-3593.

10. Caldero-Rodriguez, N. E., L. A. Ortiz-Rodriguez, A. A. Gonzalez and C. E. Crespo-Hernandez (2022) Photostability of 2,6-diaminopurine and its 2'-deoxyriboside investigated by femtosecond transient absorption spectroscopy. *Phys Chem Chem Phys* **24,** 4204-4211.

11. Crespo-Hernandez, C. E., L. Martinez-Fernandez, C. Rauer, C. Reichardt, S. Mai, M. Pollum, P. Marquetand, L. Gonzalez and I. Corral (2015) Electronic and Structural Elements That Regulate the Excited-State Dynamics in Purine Nucleobase Derivatives. *Journal of the American Chemical Society* **137,** 4368-4381.

12. Boldissar, S. and M. S. de Vries (2018) How nature covers its bases. *Phys Chem Chem Phys* **20,** 9701-9716.

13. Yamazaki, S., W. Domcke and A. L. Sobolewski (2008) Nonradiative Decay Mechanisms of the Biologically Relevant Tautomer of Guanine. *Journal of Physical Chemistry A* **112,** 11965-11968.

14. Gate, G., R. Szabla, M. R. Haggmark, J. Sponer, A. L. Sobolewski and M. S. de Vries (2019) Photodynamics of alternative DNA base isoguanine. *Phys Chem Chem Phys*.

15. Changenet-Barret, P., L. Kovacs, D. Markovitsi and T. Gustavsson (2016) Xanthines Studied via Femtosecond Fluorescence Spectroscopy. *Molecules* **21**.

16. Rottger, K., R. Stellmacher, M. C. Stuhldreier and F. Temps (2017) Ultrafast Electronic Deactivation Dynamics of Xanthosine Monophosphate. *Molecules* **22**.

17. Luhrs, D. C., J. Viallon and I. Fischer (2001) Excited state spectroscopy and dynamics of isolated adenine and 9-methyladenine. *Physical Chemistry Chemical Physics* **3,** 1827-1831.

18. Lobsiger, S., S. Blaser, R. K. Sinha, H. M. Frey and S. Leutwyler (2014) Switching on the fluorescence of 2-aminopurine by site-selective microhydration. *Nat Chem* **6,** 989-993.

19. Martinez-Fernandez, L., S. Arslancan, D. Ivashchenko, C. E. Crespo-Hernandez and I. Corral (2019) Tracking the origin of photostability in purine nucleobases: the photophysics of 2-oxopurine. *Phys Chem Chem Phys* **21,** 13467-13473.

20. Guo, X. G., Z. G. Lan and Z. X. Cao (2013) Ab initio insight into ultrafast nonadiabatic decay of hypoxanthine: keto-N7H and keto-N9H tautomers. *Physical Chemistry Chemical Physics* **15,** 10777-10782.

21. Cohen, B., P. M. Hare and B. Kohler (2003) Ultrafast excited-state dynamics of adenine and monomethylated adenines in solution: Implications for the nonradiative decay mechanism. *Journal of the American Chemical Society* **125,** 13594-13601.

22. Ullrich, S., T. Schultz, M. Z. Zgierski and A. Stolow (2004) Direct observation of electronic relaxation dynamics in adenine via time-resolved photoelectron spectroscopy. *Journal of the American Chemical Society* **126,** 2262-2263.

23. Kim, N. J., G. Jeong, Y. S. Kim, J. Sung, S. K. Kim and Y. D. Park (2000) Resonant two-photon ionization and laser induced fluorescence spectroscopy of jet-cooled adenine. *Journal of Chemical Physics* **113,** 10051-10055.

24. Kang, H., J. Chang, S. H. Lee, T. K. Ahn, N. J. Kim and S. K. Kim (2010) Excited-state lifetime of adenine near the first electronic band origin. *Journal of Chemical Physics* **133**.

25. Buchner, F., H. H. Ritze, J. Lahl and A. Lubcke (2013) Time-resolved photoelectron spectroscopy of adenine and adenosine in aqueous solution. *Physical Chemistry Chemical Physics* **15,** 11402-11408.

26. Kang, H., B. Jung and S. K. Kim (2003) Mechanism for ultrafast internal conversion of adenine. *Journal of Chemical Physics* **118,** 6717-6719.

27. Marian, C. M. (2005) A new pathway for the rapid decay of electronically excited adenine. *Journal of Chemical Physics* **122,** 10.

28. Perun, S., A. L. Sobolewski and W. Domcke (2005) Photostability of 9H-adenine: mechanisms of the radiationless deactivation of the lowest excited singlet states. *Chemical Physics* **313,** 107-112.

29. Perun, S., A. L. Sobolewski and W. Domcke (2005) Ab initio studies on the radiationless decay mechanisms of the lowest excited singlet states of 9H-adenine. *Journal of the American Chemical Society* **127,** 6257-6265.

30. Barbatti, M. and H. Lischka (2008) Nonadiabatic Deactivation of 9H-Adenine: A Comprehensive Picture Based on Mixed Quantum-Classical Dynamics. *Journal of the American Chemical Society* **130,** 6831-6839.

31. Plasser, F., R. Crespo-Otero, M. Pederzoli, J. Pittner, H. Lischka and M. Barbatti (2014) Surface Hopping Dynamics with Correlated Single-Reference Methods: 9H-Adenine as a Case Study. *J Chem Theory Comput* **10,** 1395-1405.

32. Rachofsky, E. L., J. B. A. Ross, M. Krauss and R. Osman (2001) CASSCF investigation of electronic excited states of 2-aminopurine. *Journal of Physical Chemistry A* **105,** 190-197.

33. Reichardt, C., C. W. Wen, R. A. Vogt and C. E. Crespo-Hernández (2013) Role of intersystem crossing in the fluorescence quenching of 2-aminopurine 2′-deoxyriboside in solution (vol 12, pg 1341, 2013). *Photoch. Photobio. Sci.* **12,** 2203-2203.

34. Barbatti, M. and H. Lischka (2015) Why water makes 2-aminopurine fluorescent? *Physical Chemistry Chemical Physics* **17,** 15452-15459.

35. Perun, S., A. L. Sobolewski and W. Domcke (2006) Ab initio studies of the photophysics of 2-aminopurine. *Molecular Physics* **104,** 1113-1121.

36. Evans, N. L. and S. Ullrich (2010) Wavelength Dependence of Electronic Relaxation in Isolated Adenine Using UV Femtosecond Time-Resolved Photoelectron Spectroscopy. *Journal of Physical Chemistry A* **114,** 11225-11230.

37. Szabla, R., R. W. Gora, M. Janicki and J. Sponer (2016) Photorelaxation of imidazole and adenine via electron-driven proton transfer along H2O wires. *Faraday Discussions* **195,** 237-251.

38. Gate, G., A. Williams, M. R. Haggmark, N. Svadlenak, G. Hill and M. S. de Vries (2021) Nucleobases as Molecular Fossils of Prebiotic Photochemistry: Excited-state Dynamics of C2 and C6 Substituted Purines. In *Prebiotic Photochemistry: From Urey–Miller-like*

*Experiments to Recent Findings*. (Edited by F. Saija and G. Cassone), pp. 124-147. the Royal Society of Chemistry.

39. Callahan, M. P., K. E. Smith, H. J. Cleaves, J. Ruzicka, J. C. Stern, D. P. Glavin, C. H. House and J. P. Dworkin (2011) Carbonaceous meteorites contain a wide range of extraterrestrial nucleobases. *Proc. Natl. Acad. Sci. U.S.A.* **108,** 13995-13998.

40. Miyakawa, S., H. J. Cleaves and S. L. Miller (2002) The cold origin of life: B. Implications based on pyrimidines and purines produced from frozen ammonium cyanide solutions. *Origins of Life and Evolution of the Biosphere* **32,** 209-218.

41. Sleiman, D., P. S. Garcia, M. Lagune, J. Loc'h, A. Haouz, N. Taib, P. Röthlisberger, S. Gribaldo, P. Marlière and P. A. Kaminski (2021) A third purine biosynthetic pathway encoded by aminoadenine-based viral DNA genomes. *Science* **372,** 516-+.

42. Zhou, Y., X. X. Xu, Y. F. Wei, Y. Cheng, Y. Guo, I. Khudyakov, F. L. Liu, P. He, Z. Y. Song, Z. Li, Y. Gao, E. L. Ang, H. M. Zhao, Y. Zhang and S. W. Zhao (2021) A widespread pathway for substitution of adenine by diaminopurine in phage genomes. *Science* **372,** 512-+.

43. Pezo, V., F. Jaziri, P. Y. Bourguignon, D. Louis, D. Jacobs-Sera, J. Rozenski, S. Pochet, P. Herdewijn, G. F. Hatfull, P. A. Kaminski and P. Marliere (2021) Noncanonical DNA polymerization by aminoadenine-based siphoviruses. *Science* **372,** 520-+.

44. Szabla, R., M. Zdrowowicz, P. Spisz, N. J. Green, P. Stadlbauer, H. Kruse, J. Šponer and J. Rak (2021) 2,6-diaminopurine promotes repair of DNA lesions under prebiotic conditions. *Nat Commun* **12**.

45. Gengeliczki, Z., M. P. Callahan, N. Svadlenak, C. I. Pongor, B. Sztaray, L. Meerts, D. Nachtigallova, P. Hobza, M. Barbatti, H. Lischka and M. S. de Vries (2010) Effect of substituents on the excited-state dynamics of the modified DNA bases 2,4-diaminopyrimidine and 2,6-diaminopurine. *Physical Chemistry Chemical Physics* **12,** 5375-5388.

46. Meijer, G., M. S. de Vries, H. E. Hunziker and H. R. Wendt (1990) Laser desorption jet-cooling of organic molecules. Cooling characteristics and detection sensitivity. *Applied Physics B* **51,** 395-403.

47. Siouri, F. M., S. Boldissar, J. A. Berenbeim and M. S. de Vries (2017) Excited State Dynamics of 6-Thioguanine. *J Phys Chem A* **121,** 5257-5266.

48. Grimme, S., L. Goerigk and R. F. Fink (2012) Spin-component-scaled electron correlation methods. *Wires Comput Mol Sci* **2,** 886-906.

49. Hättig, C. (2005) Structure optimizations for excited states with correlated second-order methods:: CC2 and ADC(2). *Advances in Quantum Chemistry, Vol 50* **50,** 37-60.

50. Tajti, A., L. Tulipán and P. G. Szalay (2020) Accuracy of Spin-Component Scaled ADC(2) Excitation Energies and Potential Energy Surfaces. *J Chem Theory Comput* **16,** 468-474.

51. Kruse, H., R. Szabla and J. Sponer (2020) Surprisingly broad applicability of the cc-pVnZ-F12 basis set for ground and excited states. *Journal of Chemical Physics* **152**.

52. Levine, B. G., J. D. Coe and T. J. Martinez (2008) Optimizing conical intersections without derivative coupling vectors: Application to multistate multireference second-order perturbation theory (MS-CASPT2). *Journal of Physical Chemistry B* **112,** 405-413.

53. Szabla, R., R. W. Gora and J. Sponer (2016) Ultrafast excited-state dynamics of isocytosine. *physical Chemistry Chemical Physics*.

54. Tuna, D., D. Lefrancois, L. Wolanski, S. Gozem, I. Schapiro, T. Andruniow, A. Dreuw and M. Olivucci (2015) Assessment of Approximate Coupled-Cluster and Algebraic-Diagrammatic-Construction Methods for Ground- and Excited-State Reaction Paths and the Conical-Intersection Seam of a Retinal-Chromophore Model. *J Chem Theory Comput* **11,** 5758-5781.

55. Marsili, E., A. Prlj and B. F. E. Curchod (2021) Caveat when using ADC(2) for studying the photochemistry of carbonyl-containing molecules. *Physical Chemistry Chemical Physics* **23,** 12945-12949.

56. Ahlrichs, R., M. Bar, M. Haser, H. Horn and C. Kolmel (1989) Electronic-Structure Calculations on Workstation Computers - the Program System Turbomole. *Chemical Physics Letters* **162,** 165-169.

57. Dunning, T. H. (1989) Gaussian-Basis Sets for Use in Correlated Molecular Calculations .1. The Atoms Boron through Neon and Hydrogen. *Journal of Chemical Physics* **90,** 1007-1023.

58. de Jong, W. A., R. J. Harrison and D. A. Dixon (2001) Parallel Douglas-Kroll energy and gradients in NWChem: Estimating scalar relativistic effects using Douglas-Kroll contracted basis sets. *Journal of Chemical Physics* **114,** 48-53.

59. Aquilante, F., J. Autschbach, R. K. Carlson, L. F. Chibotaru, M. G. Delcey, L. De Vico, I. F. Galván, N. Ferré, L. M. Frutos, L. Gagliardi, M. Garavelli, A. Giussani, C. E. Hoyer, G. Li Manni, H. Lischka, D. X. Ma, P. Å. Malmqvist, T. Müller, A. Nenov, M.

Olivucci, T. B. Pedersen, D. L. Peng, F. Plasser, B. Pritchard, M. Reiher, I. Rivalta, I. Schapiro, J. Segarra-Martí, M. Stenrup, D. G. Truhlar, L. Ungur, A. Valentini, S. Vancoillie, V. Veryazov, V. P. Vysotskiy, O. Weingart, F. Zapata and R. Lindh (2016) Molcas 8: New capabilities for multiconfigurational quantum chemical calculations across the periodic table. *Journal of Computational Chemistry* **37,** 506-541.

60. Haggmark, M. R., G. Gate, S. Boldissar, J. Berenbeim, A. L. Sobolewski and M. S. de Vries (2018) Evidence for competing proton-transfer and hydrogen-transfer reactions in the S-1 state of indigo. *Chemical Physics* **515,** 535-542.

61. Sobolewski, A. L., W. Domcke, C. Dedonder-Lardeux and C. Jouvet (2002) Excited-state hydrogen detachment and hydrogen transfer driven by repulsive (1)pi sigma* states: A new paradigm for nonradiative decay in aromatic biomolecules. *Physical Chemistry Chemical Physics* **4,** 1093-1100.

62. Roberts, G. M. and V. G. Stavros (2014) The role of πσ* states in the photochemistry of heteroaromatic biomolecules and their subunits: insights from gas-phase femtosecond spectroscopy. *Chem Sci* **5**.

63. Dreuw, A. and M. Wormit (2015) The algebraic diagrammatic construction scheme for the polarization propagator for the calculation of excited states. *Wiley Interdisciplinary Reviews: Computational Molecular Science* **5,** 82-95.

64. Barbatti, M., A. J. A. Aquino, J. J. Szymczak, D. Nachtigallova, P. Hobza and H. Lischka (2010) Relaxation mechanisms of UV-photoexcited DNA and RNA nucleobases. *Proc. Natl. Acad. Sci. U.S.A.* **107,** 21453-21458.

65. Oliveira, L. M. F., D. Valverde, G. J. Costa and A. C. Borin (2023) The copious photochemistry of 2,6-diaminopurine: Luminescence, triplet population, and ground state recovery. *Photochem. Photobiol.,* doi: 10.1111/php.13833

66. Schneider, M., T. Hain and I. Fischer (2009) Resonance-Enhanced Multiphoton Ionisation of Purine. *ChemPhysChem* **10,** 634-636.

67. Nachtigallova, D., M. Barbatti, J. J. Szymczak, P. Hobza and H. Lischka (2010) The photodynamics of 2,4-diaminopyrimidine in comparison with 4-aminopyrimidine: The effect of amino-substitution. *Chemical Physics Letters* **497,** 129-134.

68. Kancheva, P., D. Tuna and V. B. Delchev (2016) Comparative study of radiationless deactivation mechanisms in cytosine and 2,4-diaminopyrimidine. *J Photoch Photobio A* **321,** 266-274.

69. Lobsiger, S., R. K. Sinha, M. Trachsel and S. Leutwyler (2011) Low-lying excited states and nonradiative processes of the adenine analogues 7H-and 9H-2-aminopurine. *Journal of Chemical Physics* **134**.

70. Ismail, N., L. Blancafort, M. Olivucci, B. Kohler and M. A. Robb (2002) Ultrafast decay of electronically excited singlet cytosine via π,π* to n

π* state switch. Journal of the American Chemical Society **124,** 6818-6819.

71. Gonzalez-Vazquez, J., L. Gonzalez, E. Samoylova and T. Schultz (2009) Thymine relaxation after UV irradiation: the role of tautomerization and pi sigma* states. *Physical Chemistry Chemical Physics* **11,** 3927-3934.

72. Busker, M., M. Nispel, T. Häber, K. Kleinermanns, M. Etinski and T. Fleig (2008) Electronic and vibrational spectroscopy of 1-methylthymine and its water clusters:: The dark state survives hydration. *ChemPhysChem* **9,** 1570-1577.

73. Etinski, M., T. Fleig and C. Marian (2009) Intersystem Crossing and Characterization of Dark States in the Pyrimidine Nucleobases Uracil, Thymine, and 1-Methylthymine. *Journal of Physical Chemistry A* **113,** 11809-11816.

74. Santhosh, C. and P. C. Mishra (1991) Electronic spectra of 2-aminopurine and 2,6 diaminopurine: phototautomerism and fluorescence reabsorption. *Spectrochimica Acta A* **47,** 1685-1693.

75. Virta, P., A. Koch, M. U. Roslund, P. Mattjus, E. Kleinpeter, L. Kronberg, R. Sjoholm and K. D. Klika (2005) Synthesis, characterisation and theoretical calculations of 2,6-diaminopurine etheno derivatives. *Org Biomol Chem* **3,** 2924-2929.

76. Majoube, M., P. Millie, L. Chinsky, P. Y. Turpin and G. Vergoten (1995) Resonance Raman-Spectra for Purine. *Journal of Molecular Structure* **355,** 147-158.

77. Borin, A. C., L. Serrano-Andres, M. P. Fulscher and B. O. Roos (1999) A theoretical study of the electronic spectra of N-9 and N-7 purine tautomers. *Journal of Physical Chemistry A* **103,** 1838-1845.

78. Serrano-Andres, L., M. Merchan and A. C. Borin (2006) Adenine and 2-aminopurine: Paradigms of modern theoretical photochemistry. *Proc. Natl. Acad. Sci. U.S.A.* **103,** 8691-8696.

79. Gustavsson, T., A. Sharonov, D. Onidas and D. Markovitsi (2002) Adenine, deoxyadenosine and deoxyadenosine 5 '-monophosphate studied by femtosecond fluorescence upconversion spectroscopy. *Chemical Physics Letters* **356,** 49-54.

80. Neely, R. K., S. W. Magennis, D. T. F. Dryden and A. C. Jones (2004) Evidence of tautomerism in 2-aminopurine from fluorescence lifetime measurements. *Journal of Physical Chemistry B* **108,** 17606-17610.

81. Broo, A. (1998) A theoretical investigation of the physical reason for the very different luminescence properties of the two isomers Adenine and 2-Aminopurine. *J.Phys. Chem.* **A 102,** 526-531.

82. Miannay, F. A., T. Gustavsson, A. Banyasz and D. Markovitsi (2010) Excited-State Dynamics of dGMP Measured by Steady-State and Femtosecond Fluorescence Spectroscopy. *Journal of Physical Chemistry A* **114,** 3256-3263.

83. Karunakaran, V., K. Kleinermanns, R. Improta and S. A. Kovalenko (2009) Photoinduced Dynamics of Guanosine Monophosphate in Water from Broad-Band Transient Absorption Spectroscopy and Quantum-Chemical Calculations. *Journal of the American Chemical Society* **131,** 5839-5850.

84. Barbatti, M., J. J. Szymczak, A. J. A. Aquino, D. Nachtigallova and H. Lischka (2011) The decay mechanism of photoexcited guanine - A nonadiabatic dynamics study. *Journal of Chemical Physics* **134**.

85. Marian, C. M. (2007) The guanine tautomer puzzle: Quantum chemical investigation of ground and excited states. *Journal of Physical Chemistry A* **111,** 1545-1553.

86. Caminati, W., G. Maccaferri, P. G. Favero and L. B. Favero (1996) Free Jet Absorption Millimeter Wave Spectrum of Purine. *Chemical Physics Letters* **251,** 189-192.

87. Plützer, C., E. Nir, M. S. de Vries and K. Kleinermanns (2001) IR-UV double-resonance spectroscopy of the nucleobase adenine. *Physical Chemistry Chemical Physics* **3,** 5466-5469.

88. Plützer, C. and K. Kleinermanns (2002) Tautomers and electronic states of jet-cooled adenine investigated by double resonance spectroscopy. *Physical Chemistry Chemical Physics* **4,** 4877-4882.

89. Seefeld, K. A., C. Plützer, D. Löwenich, T. Häber, R. Linder, K. Kleinermanns, J. Tatchen and C. M. Marian (2005) Tautomers and electronic states of jet-cooled 2-aminopurine investigated by double resonance spectroscopy and theory. *Physical Chemistry Chemical Physics* **7,** 3021-3026.